AKARI, a Light to Illuminate the Misty Universe
ASP Conference Series, Vol. 418, © 2009
T. Onaka, G. J. White, T. Nakagawa, and I. Yamamura

Probing the Chemistry of Molecular Cores: 2.5–5 μm *AKARI* Grism Spectroscopy of Young Stellar Objects in B35A

Jennifer A. Noble,[1] Yuri Aikawa,[2] Helen J. Fraser,[1]
Klaus M. Pontoppidan,[3] and Itsuki Sakon[4]

[1] *Department of Physics, Scottish Universities Physics Alliance, University of Strathclyde, UK*
[2] *Department of Earth and Planetary Sciences, Graduate School of Science, Kobe University, Japan*
[3] *Division of Geological and Planetary Sciences, California Institute of Technology, USA*
[4] *Department of Astronomy, School of Science, The University of Tokyo, Japan*

Abstract. 2.5–5 μm spectra of four embedded protostars in the molecular core B35A were extracted using a novel data reduction pipeline developed for *AKARI* near infrared (NIR) grism spectroscopy. Column densities of the solid phase species present in the four lines of sight were calculated, illustrating the sensitivity of *AKARI*. The importance of ice spectra of low luminosity protostars to the development of star formation theories is discussed.

1. Introduction

The infrared spectra of protostars and young stellar objects (YSOs) embedded in molecular cores contain absorption features relating to the solid phase molecular species present in icy mantles on dust in the surrounding envelope. Previous observations have revealed a wealth of chemistry in these star-forming regions (see e.g., van Dishoeck & Blake 1998; Boogert et al. 2008; Pontoppidan et al. 2008).

The *AKARI* satellite provides an unique opportunity to measure simultaneously the absorption bands of H_2O, CO_2 and CO ice in the near infrared, specifically their stretching vibrational modes at 3.0 μm, 4.25 μm and 4.67 μm, respectively. By analysing these features we can investigate the relative ice abundances of these three fundamental species concurrently and begin to understand more explicitly the chemical networks present in molecular cores.

B35A is a well-studied molecular core in the Orion molecular cloud complex, containing a class I protostar (IRAS 05417+0907). Its relative proximity ($\sim$ 400 parsec) enables us to spatially resolve gas phase emission within the core to around 10 arc seconds. Previous observations include gas-phase studies of N_2H^+, C_3H_2 and CCS (Benson et al. 1998) and infrared emission imaging on the Spitzer space telescope (Evans et al. 2009).

This work details the reduction of *AKARI* pointings 4120022_001 and 4120-022_002 from the IMAPE project, obtained using the grism disperser in the

IRC04 spectroscopic mode. We present the spectra of objects observed in the 1′x1′ field of view (FOV), centred on IRAS 05417+0907 (hereafter referred to as Object **b**) and discuss the development of a unique data reduction pipeline to analyse *AKARI* NIR ice spectra in both the 1′x1′ and 10′x10′ FOVs. The positions of the objects presented here are shown in Figure 1. These objects were identified and classified as YSO candidates by the Spitzer Legacy program c2d (Evans et al. 2003) and are listed in Table 1.

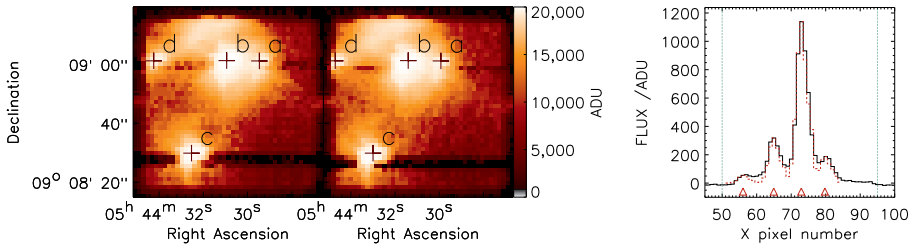

Figure 1. Left: The 4120022_001 and 4120022_002 N3 1′x1′ imaging frames showing objects in the core centred around IRAS 05417+0907 marked with crosses. Right: PSF fit (in orange) for row Y= 171 to Objects **a**,**b**,**c**,**d**, where Y is the dispersion direction and X is perpendicular to Y. The edges of the 1′x1′ FOV are marked in green (the edge effects seen in these regions result from background subtraction in the 1′x1′ FOV) and the peak positions of the PSF fits to each object are denoted by orange triangles.

2. Data Reduction and Results

Due to the presence of multiple objects in the 1′x1′ grism FOV for these pointings (see Figure 1), the official reduction pipeline was unable to accurately resolve spectra for each individual object. Thus, a novel data reduction technique has been developed.

Eight spectral frames were dark subtracted, stacked and background corrected with nearby sky. For each row (Y pixel) of the 1′x1′ FOV, the flux of each object was fitted with a point spread function (PSF) composed of two Gaussians, given by:

$$f(x) = \left[\eta_1 \cdot \exp\left\{-\left(\frac{x - X_1}{\sigma_1}\right)^2\right\} + 0.8\eta_1 \cdot \exp\left\{-\left(\frac{x - (X_1 + 2.7)}{\sigma_2}\right)^2\right\}\right] \quad (1)$$

where η_n is peak height, x is X pixel, X_n is peak position & σ_n is full width half maximum of the n^{th} Gaussian. All four objects were fitted simultaneously, as illustrated in Figure 1, with starting position of the analysis determined from c2d object coordinates. To construct a spectrum, the area under the PSF was calculated for each row of the dispersion. The flux was corrected using a spectral response function derived from *AKARI* observations of standard star K0III.

Flux corrected spectra for each object were produced by averaging spectra from the two pointings (see Figure 2). Clearly in some cases, particularly Objects

a and **d**, the photometry (shown as green diamonds) does not align with the extracted spectra. This arises due to excess emission in the region (seen in Figure 1), an issue which is currently being resolved. Some of the confusion in the official pipeline analysis arises from such excess emission. What is clear from all four spectra in that the baselines of the spectra are rising or flat i.e. all objects are YSOs, and in fact were identified as such in the c2d YSO catalogues (see Table 1). Also, three absorption bands are clearly visible: H_2O (3.0 μm, which in all cases is saturated), CO_2 (4.25 μm) and CO (4.67 μm).

Second order polynomials were fitted to points not associated with absorption features, and the resulting baselines were used to produce the optical depth spectra in Figure 3. Column densities were calculated for each object using $N = \int \tau d\nu / A$ where N is column density /cm^{-2}, A is the band strength /cm molecule^{-1} (Gerakines et al. 1995) and τ optical depth. For H_2O, $\int \tau d\nu$ was estimated using a laboratory spectrum of pure H_2O ice at T=10 K (Gerakines et al. 1995). N(CO_2) and N(CO) were calculated by summing the area under each solid phase feature. The resulting abundances are shown in Table 1.

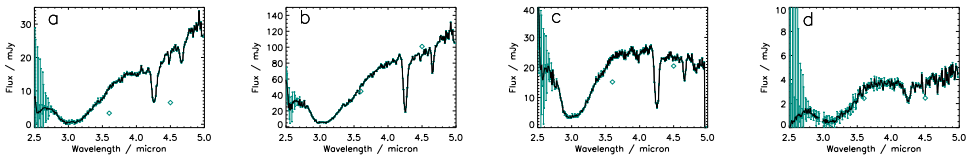

Figure 2. Flux spectra for Objects **a**,**b**,**c**,**d**. 2MASS photometric data points are marked as diamonds. Error bars are plotted (in green, in the electronic version).

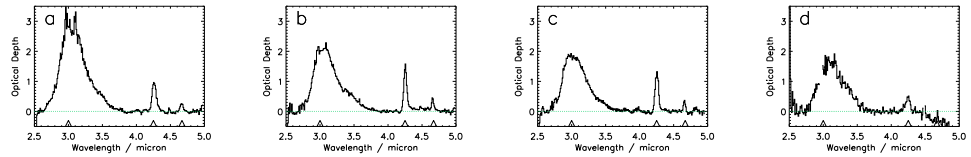

Figure 3. Optical depth spectra for Objects **a**,**b**,**c**,**d**. The expected peak frequency of H_2O, CO_2 and CO absorptions are marked with triangles at 3.0, 4.25 and 4.67 μm, respectively. Error bars are omitted for clarity.

3. Discussion and Conclusions

For the first time since ISO, both wings of the H_2O stretching mode band are seen in the *AKARI* NIR region, allowing estimation of the optical depth of the saturated H_2O ice band. In the objects presented here, the water band is saturated in at least Objects **a**,**b**,**c**, complicating the analysis. The fitting of laboratory data to the 3.0 μm band does not take into consideration the effects of scattering seen in the higher wavelength wing of the feature. The CO_2 and CO column densities presented in Table 1, calculated simply by summing the area under the feature and presented relative to that of H_2O, are shown only

Table 1. Calculated column densities

ID	Name	Object classification	N(H_2O) $10^{18}cm^{-2}$	CO_2 $\%H_2O$	CO $\%H_2O$
a	J054429.26+090856.8	YSO Class0/I[2]	6.228	8.6	9.2
b	IRAS 05417+0907	YSO[2]	3.772	16.7	22.2
c	05443085+0908260	YSO ClassII[2]	3.860	14.9	13.2
d	05443164+0908578	YSO ClassII[2]	2.807	9.7	–
	Elias 29[1]	Low Mass YSO	3.4	19.7	5.0
	Elias 16[1]	Background Star	2.5	26.0	20

[1]Column density values for a typical low-mass YSO, Elias 29 (Boogert et al. 2000), and background star, Elias 16 (Knez et al. (2005) and references therein), are shown for comparison.[2]Classification system from c2d catalogues.

for interest. Eventually fitting the H_2O band with laboratory spectra convolved with the *AKARI* PSF will result in more accurate estimates of column densities.

Low luminosity protostars are an under sampled category of class 0 objects in star forming regions. The sensitivity threshold of IRAS (0.1 $L_\odot$) resulted in the erroneous classification of many molecular cores as "starless." A survey of low luminosity embedded protostars in the Spitzer Legacy program c2d (Dunham et al. 2008) identified 50 such objects with $L_{\rm int} \leq 1.0$ $L_\odot$. Object **a** was identified as a low luminosity protostar in the c2d sample ($L_{\rm IR}$=0.141).

The details of processes which regulate accretion of mass from the envelope to the protostar are unknown (see e.g., McKee & Ostricker 2007). Models to date have underestimated the protostar population of low luminosity objects. A more full investigation of the physical and chemical properties of these objects could improve our understanding of the star formation process.

Acknowledgments. This research is based on observations with *AKARI*, a JAXA project with the participation of ESA. The authors would like to thank the Scottish Universities Physics Alliance (SUPA), the University of Strathclyde and the Japan Society for the Promotion of Science (JSPS) for funding this work.

References

Benson, P. J., Caselli, P., & Myers, P. C. 1998, ApJ, 506, 743
Boogert, A. C. A., Tielens, A. G. G. M., Ceccarelli, C., Boonman, A. M. S., van Dishoeck, E. F., Keane, J. V., Whittet, D. C. B., & de Graauw, T. 2000, A&A, 360, 683
Boogert, A. C. A., et al. 2008, ApJ, 678, 985
Dunham, M. M., Crapsi, A., Evans, N. J., II, Bourke, T. L., Huard, T. L., Myers, P. C., & Kauffmann, J. 2008, ApJS, 179, 249
Evans, N. J., II, et al. 2003, PASP, 115, 965
Evans, N. J., et al. 2009, ApJS, 181, 321
Gerakines, P. A., Schutte, W. A., Greenberg, J. M., & van Dishoeck, E. F. 1995, A&A, 296, 810
Knez, C., et al. 2005, ApJ, 635, L145
McKee, C. F. & Ostricker, E. C. 2007, ARA&A, 45, 565
Pontoppidan, K. M., et al. 2008, ApJ, 678, 1005
van Dishoeck, E. F., & Blake, G. A. 1998, ARA&A, 36, 317